PHYSICAL REVIEW B **68**, 235314 (2003)

Experimental and theoretical investigation of $Ga_{1-x}In_xAs$ surface reactivity to phosphorus

X. Wallart and C. Priester*

Institut d'Electronique de Microlectronique et de Nanotechnologie, UMR CNRS 8520, Boîte Postale 69, 59652 Villeneuve d'Ascq Cédex, France

(Received 6 March 2003; revised manuscript received 1 July 2003; published 11 December 2003)

$Ga_{1-x}In_xAs$ surfaces appear to show different behavior when exposed to phosphorus, depending on the In concentration. X-ray photoemission spectroscopy experiments provide information about phosphorus incorporation on several samples. Atomic-scale elastic energy calculations which include surface reconstructions emphasize the role or dimers for phosphorus incorporation and show a reasonable agreement for experiments that concern unstrained surfaces. Another roughening mechanism is proposed for strained surfaces.

DOI: 10.1103/PhysRevB.68.235314 PACS number(s): 82.45.Jn, 81.05.Ea, 81.65.−b, 82.80.Pv

I. INTRODUCTION

Heterostructures involving both arsenic and phosphorus based III-V semiconductors are of interest for optoelectronic as well as for microelectronic applications. However, the epitaxial growth of these structures with abrupt interfaces still remains a challenge whatever the growth technique used, i.e., metalorganic vapor phase epitaxy (MOVPE) or molecular-beam epitaxy (MBE).[1,2] Indeed, without any particular care, the resulting interfaces are diffuse with significant anion intermixing, due to various "memory effects" in the growth system, related to the anion overpressure during growth and to the high vapor pressure of arsenic and phosphorus.[3–8] Both interfaces do not behave symmetrically since As is more easily incorporated in a phosphide overlayer than P in an arsenide one.[9] The preferred recipe for reducing anion intermixing involves a growth interruption at the interface during which the arsenide surface is exposed for a given time to a phosphorus flux or vice versa.[10–13] A tradeoff has to be found for the best value of this exposure time which must be long enough to allow a good anion commutation but without degrading the interface quality.

This kind of procedure then raises the question of the reactivity of an arsenide surface to a phosphorus flux and of a phosphide surface to an arsenic flux. The most extensively studied case is that of InP under an As pressure since it occurs directly when people make the InP substrate oxide removal under an As overpressure.[14] In this case, it has been shown that a thin InAs layer around 2 ML (monolayers) thick is formed at the surface.[15] The As/P exchange reaction at the InP (001) surface versus substrate temperature has recently been investigated and the surface phase diagram has been determined, confirming that the substitution of As for P is limited to the two or three outermost monolayers.[16] On the same surface, Yoon *et al.*[17] and Yang *et al.*[18] have studied the influence of the V/III ratio or of the surface reconstruction on the formation of three-dimensional structures during As/P exchange reaction. As regards GaAs surfaces, Jönsson *et al.*[19] have shown that a MOVPE grown As-rich $c(4\times4)$ GaAs surface reacts with PH_3 to form a single-layer P-terminated structure for temperatures below 600 °C. They have observed that this structure is not stable at higher temperatures leading to surface roughening at 650 °C. This trend has been noted by Mahalingham *et al.*[20] from TEM observations on InGaP/GaAs superlattices. From photoluminescence measurements, Aurand *et al.*[21] have shown that a GaP-rich layer up to 2 ML thick is formed at the GaAs surface when exposed to cracked phosphine for a few tens of seconds. Nevertheless, very few is reported on the reactivity of an InAs surface exposed to a phosphorus flux.

In order to minimize the As incorporation in phosphides, the exposure of arsenides to phosphorus prior to the growth of a phosphide layer is required. That is why we have studied the surface reactivity of $Ga_{1-x}In_xAs$ alloys to a phosphorus flux. For a 500 °C substrate temperature, we find that, except for the InAs case ($x=1$), the surface roughens rather rapidly and that roughening occurs faster in the alloy case than in the GaAs one ($x=0$). We show that these observations cannot be attributed to different amounts of phosphorus incorporated in the layer, as determined by x-ray photoelectron spectroscopy (XPS). Using valence force field calculations and taking properly into account the surface reconstruction, we show that the difference between GaAs and InAs is related to the elastic energy differences occurring upon phosphorus incorporation in both systems. For the alloys, we show that, in the case of an average alloy matched to its substrate, the surface reconstruction, mainly dimers, induces some alloy ordering in the atomic layers very close to the surface, which renders less favorable phosphorus incorporation (above half a monolayer) as far as surface keeps flat.

II. EXPERIMENTAL

Samples are grown by gas source molecular-beam epitaxy in a Riber 32P reactor, using standard effusion cells for the elements III and cracked phosphine and arsine on undoped GaAs(001), InAs(001), and Fe-doped InP(001) substrates. We consider $Ga_{1-x}In_xAs$ alloys with four different In concentrations: $x=0$ (sample X0), 0.2 (sample X20), 0.53 (sample X53) and 1.0 (sample X100). The X0 sample is a 4000-Å-thick buffer layer grown at 630 °C on GaAs. For the X20 sample, we grow the same buffer layer followed by the growth of a 100 Å strained $Ga_{0.8}In_{0.2}As$ layer at 500 °C. The X53 sample is a 1000-Å-thick lattice-matched $Ga_{0.47}In_{0.53}As$ layer grown at 500 °C on a 2000-Å-thick InP buffer layer. Finally, the X100 sample is a 4000-Å-thick InAs buffer grown at 500 °C on InAs. The growth rate for all samples lies in the 0.7–1.0 ML/s. range. After growth, the samples

 ©2003 The American Physical Society

exhibit a clear (2×4) (samples X0, X53, and X100) or (2×3) (sample X20) reflection high-energy electron-diffraction (RHEED) pattern, characteristic of As-rich surfaces. Then the InAs and the alloy samples are kept under an arsenic flux for 2 min to allow surface smoothing before the exposure to the phosphorus flux. On the contrary, GaAs samples are cooled down to 500 °C, the arsenic flux being interrupted below 550 °C to preserve the (2x4) reconstruction, before the phosphorus exposure [3-SCCM phosphine flow rate) at 500 °C. Following this procedure, the (2×4) GaAs surface is $\beta2$ type[22] whereas the InAs one is probably a mixture between $\alpha2$ and $\beta2$ structures.[23] As regards the alloys, the (2×4) reconstruction occurring for sample X53 is probably closed to that of InAs due to In segregation, leading to an In-rich topmost layer. For the X20 sample, the observed (2×3) reconstruction has been described elsewhere.[24,25] For all samples, during the cooling down to room temperature, the phosphorus flux is interrupted when the substrate temperature reaches 400 °C to avoid any phosphorus accumulation at the surface and the RHEED pattern is monitored to ensure it remains unchanged. We perform XPS measurements on some of the samples by transferring them to the XPS chamber connected under UHV to the growth chamber. The XPS system is a Physical Electronics model 5600, modified by SINVACO in order to analyze 3-inch MBE samples. We use a monochromatic Al $K\alpha$ x-ray source and an analyzer pass energy of 12 eV. Under these conditions, the overall resolution as measured from the full width at half maximum of the Ag 3d5/2 line is 0.55 eV. The acceptance angle of the analyzer is set to 14° and the angle between the incident x rays and the analyzer is 90°. The direction of photoelectrons is given by the polar angle θ, as referenced to the sample surface. To obtain angle-dependent XPS results, the polar angle is varied from 25° to 75°. The intensity of the various XPS core levels (CL's) is measured as the peak area after standard background subtraction according to the Shirley procedure.[26] Photodiffraction effects are often prominent on single crystals[27] and, as they superimpose to the XPS signal variations relative to the concentration gradient, they can make concentration profile determination rather difficult. To minimize these effects, we perform an average of the different XPS core level intensities with respect to the azimuth.[28] Then, we calculate intensity ratios between the P $2p$ and As $3d$ CL's with close binding energies.[29] For the CL decomposition, we apply the deconvolution procedure proposed by Joyce *et al.*[30] In this procedure, the As $3d$ CL is synthesized using Voigt functions by a doublet for the 3/2 and 5/2 components whereas the P $2p$ CL is modeled by a doublet for the 1/2 and 3/2 components. The branching ratios are theoretical ones and the splitting energies are fixed at 0.69 eV between As $3d_{3/2}$ and As $3d_{5/2}$ and 0.85 eV between P $2p_{1/2}$ and P $2p_{3/2}$, which are typical values for these core levels.[31] The best fit is obtained through a least-square minimization procedure. The surface components are modeled with the same parameters than the bulk component, i.e., the Gaussian and Lorentzian broadening are kept fixed for each component of a given CL. This broadening is chosen as that obtained on (2×4) GaAs and InP surfaces analyzed in the same conditions. Finally, samples have been examined "*ex situ*" by atomic force microscopy (AFM), using a Digital Nanoscope III, working in the tapping mode.

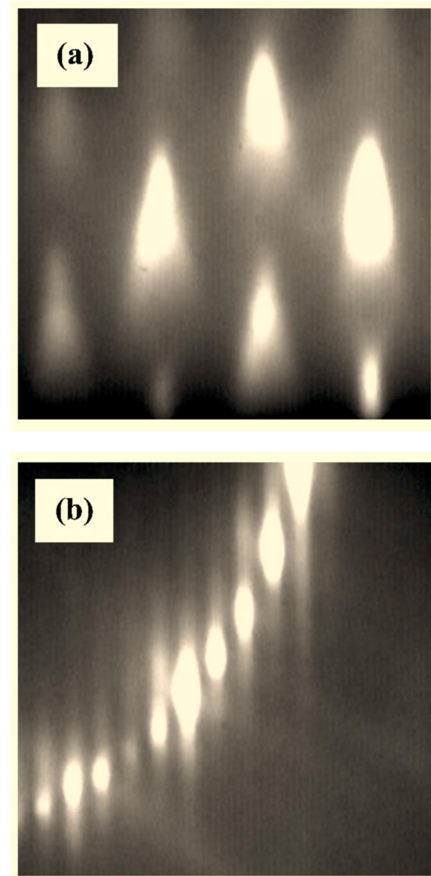

FIG. 1. RHEED patterns along the [110] azimuth of a (2×4) GaAs surface exposed for 5 min (a) and of a (2×4) InAs surface exposed for 10 min (b) to a cracked phosphine flux (3 SCCM) at 500 °C.

III. RESULTS

A. RHEED and AFM observations

Upon exposure to a 3-SCCM phosphine flow rate at 500 °C, for all samples except the InAs one, the starting RHEED pattern [(2×4) for samples X0 and X53, (2×3) for sample X20] is progressively lost with the appearance of arrow-headed shape spots in the [110] azimuth. This indicates that the surface roughens as exposure goes on, resulting in a spotty pattern after a few minutes [Fig. 1(a)]. As revealed by the evolution of the intensity of a three-dimensional (3D) Bragg spot (Fig. 2), roughening occurs more rapidly for the alloys (after roughly a 10-s exposure time) than for GaAs (after 70 s). In the same way, the transition from a 2D to 3D morphology is more abrupt for the X53 sample than for the X20 one. On the contrary, for the InAs sample, the RHEED pattern indicates that the reconstruction first starts as (2×4), then changes towards (2×2) after 30 s exposure and turns back towards a (2×4) pattern after 60 s. This pattern [Fig. 1(b)] is characterized by intermediate streaks as bright as the main ones in the [110]

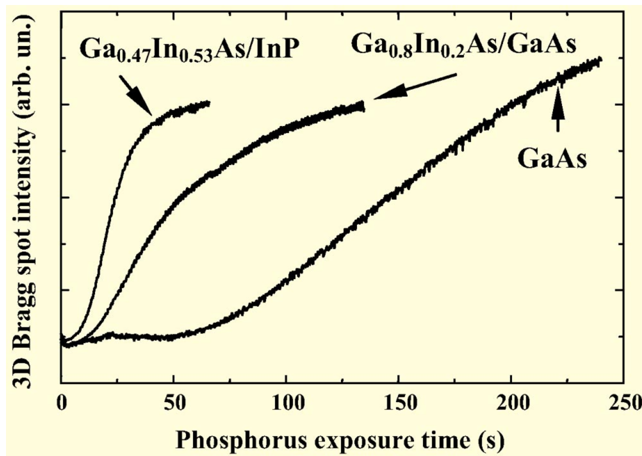

FIG. 2. 3D Bragg spot intensity evolution vs exposure time to a cracked phosphine flux (3 SCCM) at 500 °C for a (2×4) GaAs, a (2×3) $Ga_{0.8}In_{0.2}As$, and a (2×4) $Ga_{0.47}In_{0.53}As$ surfaces.

azimuth and is similar to that observed on a (2×4) InP surface. In this case, we never detect any trend to a surface roughening until 30 min exposure time which is the longest we explore in this work.

When increasing the substrate temperature to 600 °C or 650 °C for the X0 sample (GaAs), surface roughening tends to occur more rapidly than at 500 °C.

On the other hand, when decreasing the substrate temperature to 450 °C during the phosphorus exposure, samples X20 and X53 do not exhibit anymore a tendency to surface roughening. In this case, the starting reconstruction under As stabilization is a (1×3)–(4×3) one for both alloys. Upon P exposure, this reconstruction vanishes within 10 s and turns to a (3×4) for sample X53 and to a (3×2) for sample X20 after roughly 40 s. When P exposure goes on, the RHEED pattern keeps its 2D character for times as long as 10 min.

These findings are confirmed by the AFM observations. They clearly evidence that the InAs surface is still smooth with clearly visible atomic steps [Fig. 3(d)] after rather long exposure times (10 min). On the contrary, for the other samples, the surface becomes rough with small dots formation [Fig. 3(a–c)], even after short exposure times (a few tens of seconds). These observations indicate in which range kinetic limitations are ruling out surface roughening. In this paper we will mainly focus on experiments at 500 °C or more, for which the near equilibrium conditions are fulfilled.

B. XPS measurements

In light of the above observations, upon phosphorus exposure, the surface morphology evolution seems to depend on the sample composition. That is why we determine the incorporated phosphorus in different samples before the onset of roughening by XPS measurements. We perform them on X0 after 60-s exposure, on X20 and X53 after 10 s, and on X100 after 1-, 10-, and 30-min exposure at 500 °C. For X20, we also get XPS spectra after 5-min exposure at 450 °C. Figure 4 shows the measured intensity ratios be-

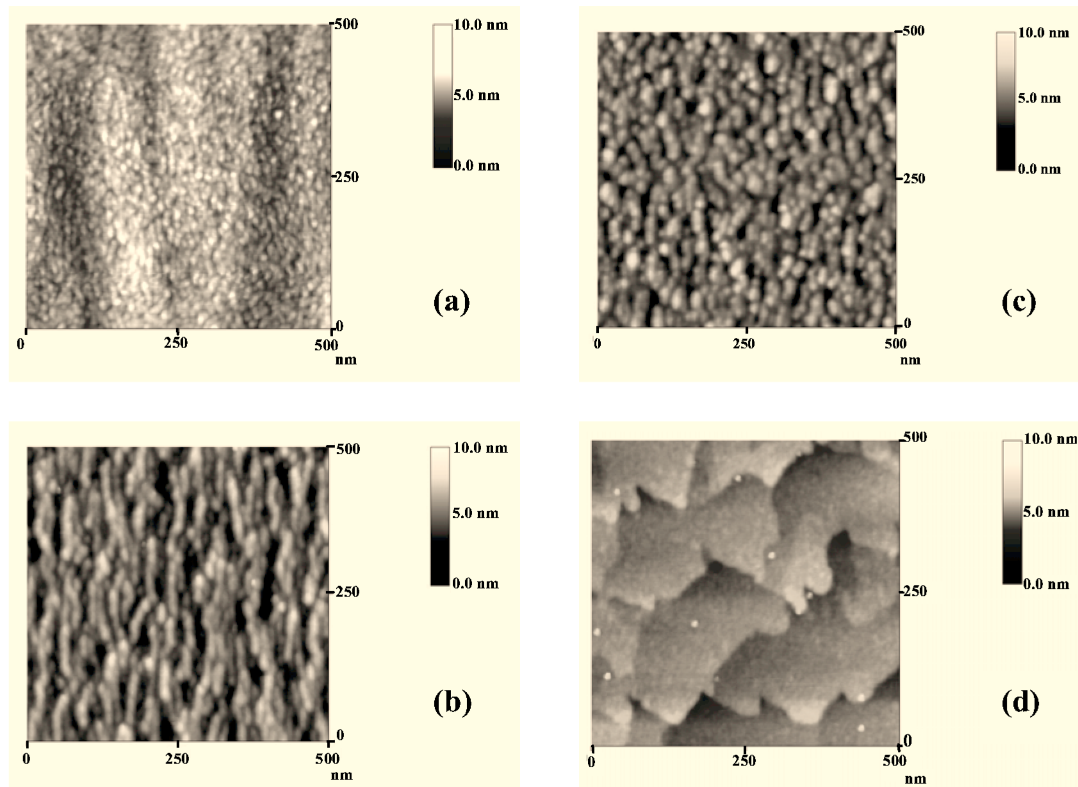

FIG. 3. AFM images of a (2×4) GaAs surface exposed for 5 min (a), of a (2×3) $In_{0.2}Ga_{0.8}As$ one exposed for 3 min (b) of a (2 ×4) $In_{0.53}Ga_{0.47}As$ one exposed for 3 min (c), and of a (2×4) InAs one exposed for 10 min (d) to a cracked phosphine flux (3 SCCM) at 500 °C.

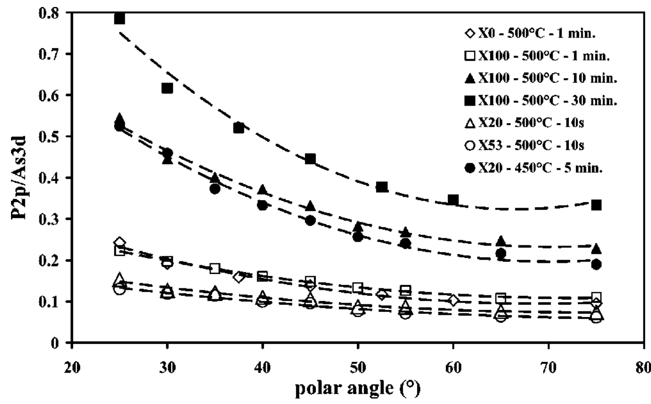

FIG. 4. P $2p$/As $3d$ XPS intensity ratios vs the detection polar angle with respect to the surface plane for samples X0 (GaAs), X20 ($In_{0.2}Ga_{0.8}As$), X53 ($Ga_{0.53}In_{0.47}As$), and X100 (InAs) exposed to a cracked phosphine flux (3 SCCM) at 450 °C or 500 °C.

tween the P $2p$ and As $3d$ CL's versus the detection polar angle with respect to the surface plane. The decrease of these ratios with increasing angle clearly indicates that phosphorus is mainly located near the sample surface and does not penetrate very deep in the sample. However, the P $2p$ CL does not exhibit the high binding-energy component (≈ 1 eV shifted from the main one) characteristic of elemental phosphorus on both InP and GaP surfaces.[32,33] This indicates that there is no phosphorus accumulation at the surface during the cooling down of the sample. From Fig. 4, at 500 °C, it is obvious that the amount of phosphorus in the X0 (GaAs) and X100 (InAs) samples after 60-s exposure is quite similar whereas it is smaller for the X20 and X53 samples after 10-s exposure.

From these experimental curves, it is possible to get an estimate of the amount of phosphorus in the sample although it is not possible to recover a unique concentration profile inside the sample, since different concentration profiles can lead to a rather similar agreement with the experiment. Then it is necessary to assume the composition profile *a priori* and to calculate the related intensity ratios. For sake of simplicity, we use a square profile with a constant phosphorus concentration on a given depth. For estimating the relative sensitivity factor between As $3d$ and P $2p$ CL's, we use MBE grown (2×4) GaAs and P-rich (2×4) GaP surfaces which present very close surface compositions although their atomic structures could differ.[33,34] Moreover, XPS data are recorded at normal emission from the surface in order to minimize surface effects. The most relevant quantity is the incorporated phosphorus amount, i.e., the total amount minus the phosphorus amount lying in the outermost atomic plane, this latter being too sensitive to the cooling down procedure to be meaningful. Since the determination of the incorporated P amount is not straightforward, we use the two different methods described below.

In the first method, we first try to get an estimate of the incorporated P amount by using the total As $3d$ and P $2p$ XPS intensities. We model the P $2p$/As $3d$ intensity ratios using a square concentration profile. The results of the fit are given in Table I, columns 3, c(P), and 4 d(P), first line for each sample. To interpret these results, we then consider two extreme cases. (i) in the first one, we assume that the surface is terminated by a complete anion atomic plane (which is then the outermost atomic plane); (ii) in the second one, we assume that the surface is terminated by a complete cation plane (the first anion plane is then the second atomic plane from the surface). For the anion-terminated surface, d(P) includes the phosphorus of the outermost anion plane which we do not consider as incorporated. The incorporated P amount is obtained by $c(\mathrm{P})*[d(P)-1]$ which gives the lower value of the range reported in column 5 in Table I. On the contrary, for the cation-terminated surface, the incorporated P amount is calculated via $d(\mathrm{P})*c(\mathrm{P})$, which gives the higher value of the range in column 5. Of course the actual surface is in between these two extreme cases and that is

TABLE I. Phosphorus concentration c(P) and in-depth penetration d(P) as deduced from XPS measurements according either to the total P $2p$ and As $3d$ intensities or to the bulk components extracted from the decomposition of the CL's.

Sample	Method	c(P)	d(P) : in-depth P penetration (ML)	Total amount of incorporated P (ML)
GaAs—500 °C	Total intensities	0.48	3	0.96–1.44
1 min	Bulk component intensities	0.55	2	1.10
InAs—500 °C	Total intensities	0.48	3	0.96−1.44
1 min	Bulk component intensities	0.58	2	1.16
InAs—500 °C	Total intensities	0.68	4	2.02−2.72
10 min	Bulk component intensities	0.77	3	2.31
InAs—500 °C	Total intensities	0.72	5	2.88−3.60
30 min	Bulk component intensities	0.84	4	3.36
$Ga_{0.8}In_{0.2}As$	total intensities	0.36	3	0.72−1.08
500 °C—10 s	Bulk component intensities	0.46	2	0.92
$Ga_{0.47}In_{0.53}As$	Total intensities	0.32	3	0.64−0.96
500 °C—10 s	Bulk component intensities	0.37	2	0.74
$Ga_{0.8}In_{0.2}As$	Total intensities	0.84	3	1.68−2.52
450 °C—10 s	Bulk component intensities	0.96	2	1.92

why this first method only provides a lower and a higher estimate of the incorporated P amount.

To get more precise results, we use a second method in which we decompose the P $2p$ and As $3d$ CL's in their bulk and surface components. We assume that the surface components are related to nonincorporated P and As, i.e., to P and As atoms which are located on the outermost atomic plane whereas the bulk components are related to As and P atoms located on the second anion atomic plane or deeper. In the CL's decomposition, we assume two surface components as previously done for GaAs surfaces[31] and for P-rich phosphide surfaces.[32,33] Figure 5 shows a typical decomposition of the P $2p$ and As $3d$ CLs. Doing so, for a 30 min exposure time of the X100 sample, we only need one surface component for the P $2p$ CL at lower binding energy as in the pure (2×4) InP surface case.[32,35] Then, after long P exposure times, the P $2p$ CL of the InAs surface becomes very close to that recorded on an InP (2×4) one, confirming the similarity observed in the RHEED patterns. Then we model the P $2p$ and As $3d$ bulk component intensity ratios by a square concentration profile. The results of the fit are given in Table I, columns 3, $c(\mathrm{P})$, and 4, $d(\mathrm{P})$, second line for each sample. This method allows us to get a more precise value of the incorporated P amount, reported in column 5

It is clear from Table I that the observed different behavior from the roughening point of view between X0 (GaAs) and X100 (InAs) at 500 °C cannot be accounted for by a significant difference in the amount of incorporated phosphorus. In the same way, the incorporated phosphorus amount before the onset of roughening is significantly lower in the X20 and X53 samples than in the X0 sample. On the contrary, for sample X100 after 30-min exposure for which the surface is still 2D, the incorporated phosphorus amount is considerably larger than that determined before the onset of roughening on sample X0 (GaAs). This implies that the tendency to surface roughening upon phosphorus exposure cannot be directly related to a more or less important amount of incorporated phosphorus. Finally, we can also note the effect of the growth temperature since for sample X20, at 450 °C, no surface roughening is observed after incorporation of 2-ML phosphorus whereas at 500 °C, surface roughening occurs for less than 1-ML incorporated phosphorus.

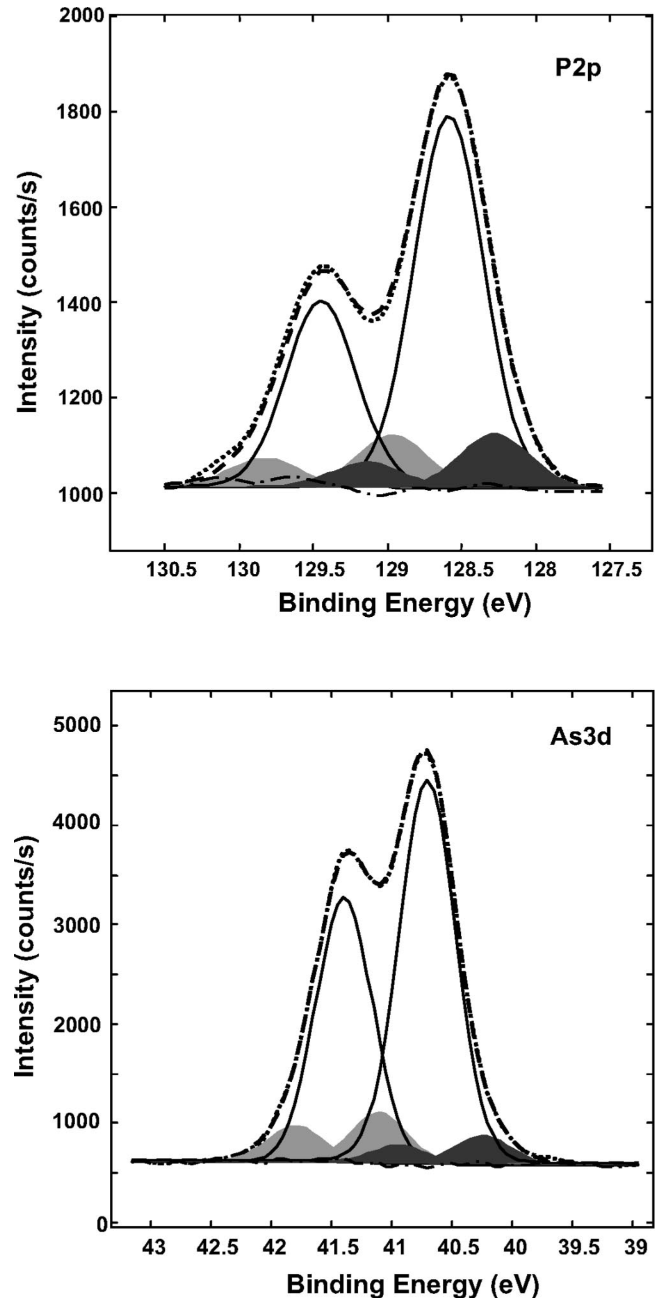

FIG. 5. Typical XPS core-level decomposition for P $2p$ and As $3d$ (sample InAs after 1-min exposure time at 500°C). The takeoff angle of the photoelectrons is 25° with respect to the surface plane. Shaded areas indicate surface components, the full lines are related to the bulk one, the dashed line is the resulting fit, the dotted line is the experimental data, and the dashed-dotted line is the residual of the fit.

IV. MODEL AND DISCUSSIONS

As the amount of incorporated phosphorus definitely cannot be the key parameter for the roughening onset, let us now consider the strain induced by phosphorus incorporation. For the samples under investigation here, the phosphorus incorporation tends either to induce a tensile strain in the surface layer (for samples X0, X53, and X100) or to reduce the initial compressive strain (for sample X20). For a given distribution of incorporated phosphorus, the mean induced tensile strain is similar for X0, X53, and X100 samples. Taking into account the amount of phosphorus incorporated in X0, X53, and X100 samples determined above, it is clear that the surface roughening of X0 and X53 samples cannot be explained by the mean induced tensile strain since X100 sample should exhibit surface roughening too, which is not the case. In the same way, this argument cannot account for earlier roughening on sample X53 than on X0 sample. Clearly, a more detailed picture is needed.

When looking at an atomistic picture of the surface layer, one important feature to consider is the tendency of the quaternary GaInAsP alloys to exhibit spinodal decomposition[36–38] to form GaP and InAs-rich regions. Considering thermodynamical calculations on spinodal decomposition

reported by LaPierre *et al.*[36,37] could be useful here for sample X53 for which the incorporation of phosphorus leads the resulting quaternary to fall inside the miscibility gap. However, the same calculations predict that the quaternary formed by P incorporation in the X20 sample falls mainly outside the miscibility gap and do not predict any miscibility gap for GaAsP. Then it is not possible to explain our results by a thermodynamic description of the spinodal decomposition even if this decomposition is indeed an important factor to be considered. Moreover, as outlined by LaPierre *et al.*,[36,37] the origin of the phase separation observed during the growth of the quaternary GaInAsP alloys is probably surface related and not a bulk effect. That is why we model the systems from a microscopic point of view, taking into account the surface reconstruction. Let us first present the results relative to the two binaries GaAs and InAs.

A. GaAs and InAs cases

Since growth roughening is often related to the elastic energy of the system, we describe the two systems we are interested in by means of a valence force field model. We choose, as in Ref. 39, a Keating's description,[40] and the parameters for GaAs, GaP, InAs, and InP are those of Ref. 41. In our experiments, the elastic energy increase is due to the replacement of As atoms by P ones. Thus we first calculate the substitutional energy of P atoms in GaAs or InAs assuming various surface reconstructions. First the simple and academic cases of (2×1) anion-rich and (1×2) cation rich are considered, as they are very helpful for enlightening the dimer role. For the anion-rich surfaces that present a (2×4) reconstruction, we only display results for the $\beta2(2\times4)$ as we have checked that an $\alpha2(2\times4)$ leads to similar results; this is due to equivalent surface corrugation and a great amount of inequivalent α- and β-type sites in the upper plane. As far as corrugation is concerned, our calculations clearly demonstrate that this short-range corrugation is less efficient than dimers: phosphorus incorporates below ridges as well as below trenches. The key parameter is definitely the presence of dimers: for a (2x1) anion-rich surface [Fig. 6(a)], due to the presence of anion dimers, two different sites, α (below dimers) or β (between dimers), occur on the anion plane just below the surface. As shown in Fig. 7, these two sites present a large difference in substitutional energy, in agreement with previous work.[39] For a (1×2) cation-rich surface [Fig. 6(b)], the inequivalent α and β sites are located in the second anion plane below the surface whereas for the $\beta2$ (2×4) surface (not represented in Fig. 6), one gets several different α-type and β-type sites located in the two upper planes below the surface.

The calculated substitutional energy is roughly twice as large in GaAs (average value—45 meV/solute atom) than in InAs (25 meV/solute atom). This is mainly due to the bond strength difference between GaP and InP which is also at the origin of the difference between the interaction parameter Ω involved in the calculation of the alloys mixing enthalpy (for GaAsP, the mean value of Ω is 35 meV (Ref. 42) whereas it is 15 meV for InAsP (Ref. 43).

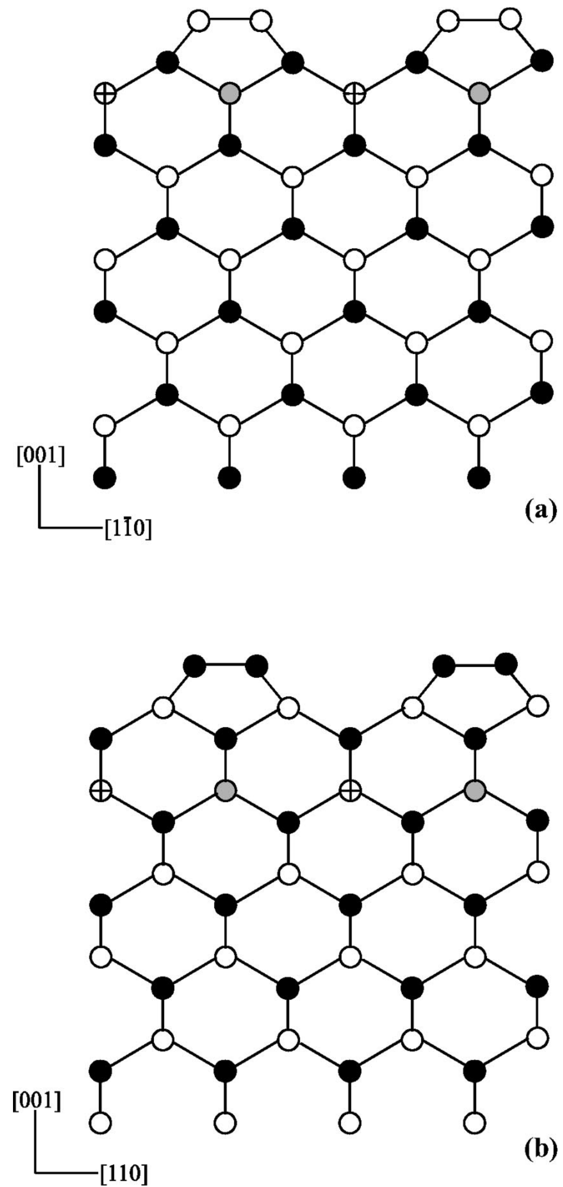

FIG. 6. Schematic drawing showing the existence of α and β sites for the incorporation of phosphorus in the second anion plane from the surface either for an anion-rich (2×1) reconstruction (a) or for a (1×2) cation-rich one (b). Filled circles are for cations, opened ones are for anions, gray ones are for the α sites, and the crossed ones for the β sites.

Nevertheless, the observed difference in substitutional energy is not sufficient to explain our experimental evidences since it considers only one single P atom in a GaAs or InAs matrix whereas, for a greater amount of incorporated phosphorus, elastic interaction between P atoms is efficient and needs to be taken into account. To go further, we perform the elastic energy calculation for a given amount of incorporated phosphorus on a definite depth. In Figs. 8 and 9, we plot the energy difference between the system with and without phosphorus incorporation for the (2×1) and (2×4) reconstructions, respectively. For these calculations, guided by the XPS results, we focus on an incorporated phosphorus amount ranging from 0.5 to 2 ML and extending 2 or 3 ML from the

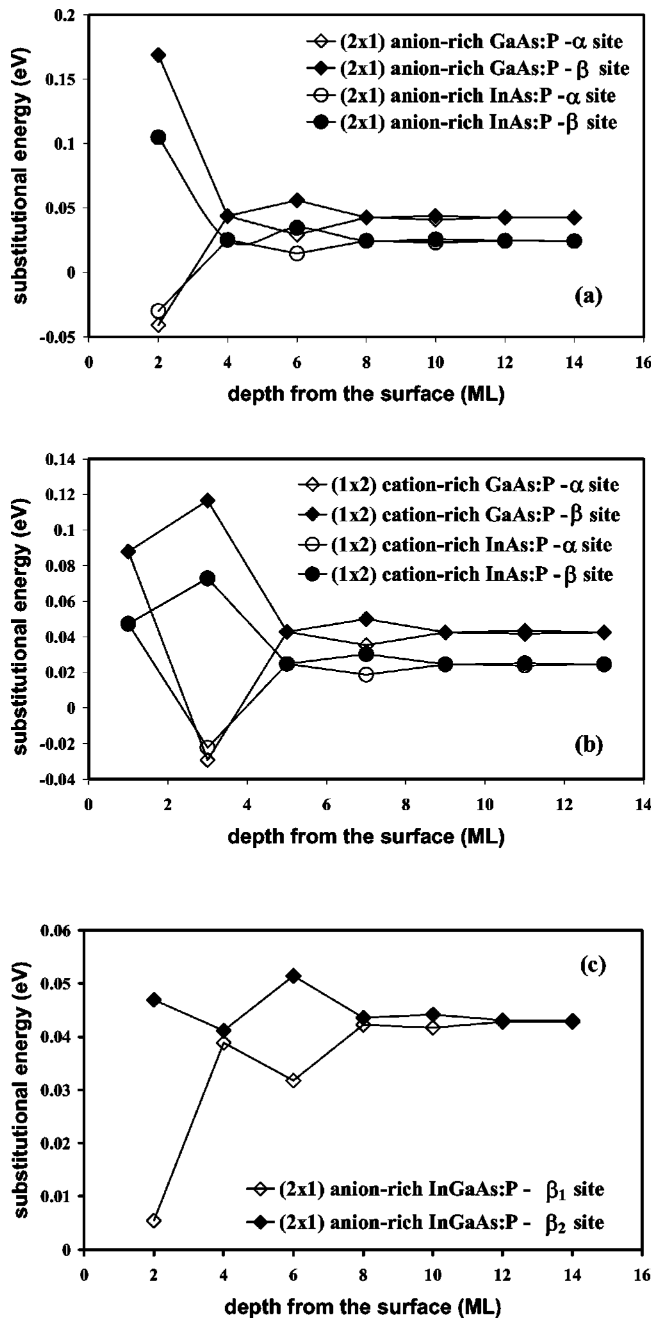

FIG. 7. Substitutional energy of P atoms in GaAs and InAs matrix, considering either an anion-rich (2×1) reconstruction (a) or a cation-rich (1×2) one (b), and in a $In_{0.5}Ga_{0.5}As$ one for a (2×1) anion-rich reconstruction (c).

surface. The distribution of P atoms within the allowed two or three atomic planes is got by minimizing the elastic energy of the system. Once again, energies are roughly twice as large in GaAs than in InAs. Moreover, in Fig. 9, one can note a rapid increase in the energy difference above 1.2 ML incorporated phosphorus in the sample, if a two plane extension is considered. This increase corresponds to P atoms starting to occupy less favorable (β-type) sites. This 1.2-ML value is in good agreement with the above XPS determination of the phosphorus amount incorporated just before the onset of roughening on GaAs (1.1 ML). Within this model,

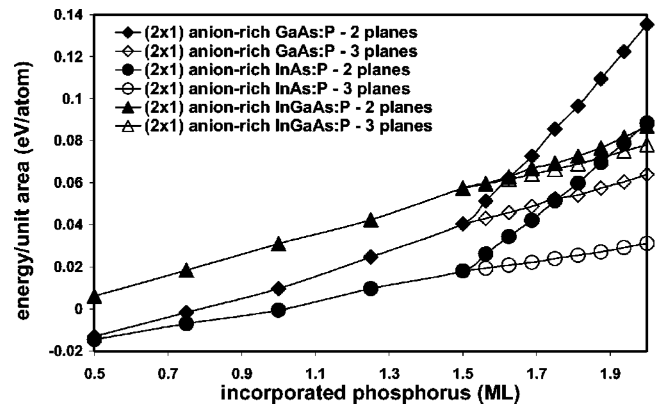

FIG. 8. Elastic energy differences between the systems with and without phosphorus for GaAs, InAs, and $Ga_{0.5}In_{0.5}As$ considering a (2×1) reconstruction and assuming phosphorus incorporation on two or three atomic planes below the surface.

we can infer that P incorporation occurs first on the most favorable sites (α type) of the first plane below the surface and on the equivalent sites of the second plane below the surface. Then, since diffusion is very weak in III-V semiconductors at 500 °C, the in-depth penetration of P is kinetically limited and P incorporation goes on with the occupation of the less favorable sites (β type) of the first plane under the surface. This leads to an important increase of the elastic energy, especially in the GaAs case, which in turn would explain the relaxation via surface roughening.

B. Alloy cases

In this case, we have first to examine the surface dimer effect on the cation distribution. Indeed, for the (1×2) cation-rich surface, we have shown above [Figs. 6(b) and 7(b)] that the presence of surface cation dimers leads to two inequivalent sites for P incorporation in the second anion plane from the surface (α site below the dimers, β site between the dimers). In the same way, for an anion-rich alloy surface, the presence of the anion dimers will lead to two inequivalent sites for the Ga atoms in the second cation plane

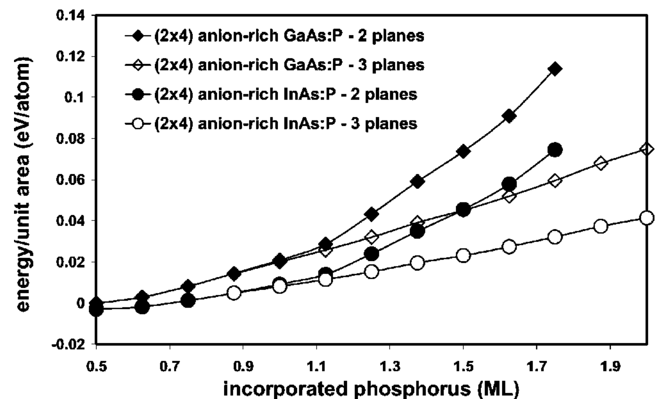

FIG. 9. Elastic energy differences between the systems with and without phosphorus for GaAs and InAs considering a (2×4) reconstruction and assuming phosphorus incorporation on two or three atomic planes below the surface.

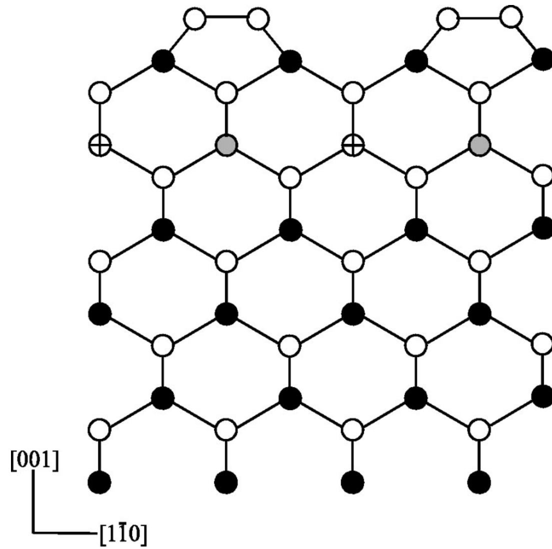

FIG. 10. Schematic drawing showing the existence of α and β sites for the Ga atoms in the second cation layer from the surface of $In_{0.5}Ga_{0.5}As$ due to the presence of As dimers. Filled circles are for cations, opened ones are for anions, gray ones are for the α sites, and the crossed ones for the β sites.

from the surface: a favorable one (α site) below the dimers and a more energetic one (β site) between the dimers (Fig. 10). This implies that the second cation plane will present a kind of ordering due to the anion dimers with Ga atoms preferentially below the dimers and In atoms preferentially between the dimers.[44] XPS Ga $3d$-In $4d$ spectra recorded at 25° and 75° polar angles reveal a significant In $4d$ surface component associated with In segregation as observed in a previous work.[29] Then, in our model, in order to take into account In segregation towards the surface, the upper cation plane (where all sites are equivalent) is supposed to be purely In. For simplicity, as far as X53 sample is concerned, we assume that all other cation planes contain half In and half Ga atoms. In such a dimer induced surface ordered alloy, how altered are α and β sites for phosphorus incorporation? β sites keep repulsive, but a bit less repulsive than in binaries, as phosphorus incorporation will induce InP areas, obviously lattice matched to the InP substrate. This can be viewed in Fig. 7(c): β site substitution energy in the first layer is significantly lower in the alloy than in the binaries [Fig. 7(a)]. On the other hand, the sites located below the dimer rows are no longer attractive from phosphorus incorporation point of view, but become slightly repulsive, as incorporating P atoms in these sites creates lines of GaP bonds (Fig. 10), which are 7% mismatched to the substrate. Subsurface anion sites are thus never α type, but slightly (β_1) or strongly (β_2) β type: that's why the phosphorus incorporation curves for a 2×1 anion-rich surface displayed in Fig. 8 show InGaAs curves (triangles) lying significantly upper than both InAs (circles) and GaAs (diamonds) curves. This is the basic mechanism which explains why X53 roughens earlier than X0. If one turns to a more realistic 2×4 surface, surface cation ordering is a bit more complicated and InGaAs phosphorus incorporation curves lie clearly upper than GaAs curves only if one takes into account some In

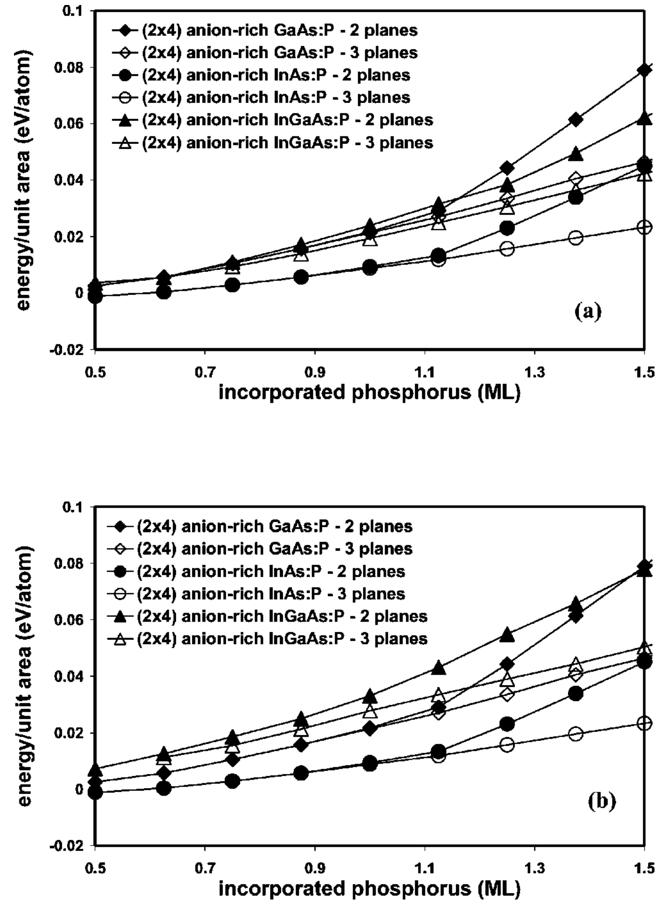

FIG. 11. Elastic energy differences between the systems with and without phosphorus for GaAs, InAs, and $In_{0.5}Ga_{0.5}As$ considering (2×4) reconstruction and the nominal In concentration in the second cation plane (a) and a slightly In depleted second cation plane (b).

depletion just below the In surface plane: Fig. 11(a) corresponds to the nominal In concentration in the second cation plane and Fig. 11(b) to an In depleted second cation plane (three In atoms and five Ga atoms in the surface unit cell). Under this assumption, the calculated phosphorus incorporation curves are in reasonable agreement with the experimental observation of the roughening of unstrained GaAs, InAs, and $Ga_{0.47}In_{0.53}As$ surface under phosphorus exposition.

These three systems are lattice matched to their substrate before incorporating phosphorus. This is not the case for $Ga_{0.8}In_{0.2}As$ on GaAs substrate. In this latter system indeed, phosphorus incorporation first tends to lower the mean strain in the alloy. This explains why, at low phosphorus exposure temperatures (450 °C), a rather great amount of phosphorus is incorporated very fast near the surface, as reported in Table I. For this reason, one would expect that, at usual phosphorus exposure temperatures, $Ga_{0.80}In_{0.20}As$ would roughen later than GaAs. That is what the model shows if one calculates the equivalent of Fig. 11 for this strained alloy: either one considers a $\beta2$ 2×4 reconstruction or the more realistic (2×3) (which also exhibits surface anion dimers, as shown in Ref. 25), the $Ga_{0.8}In_{0.2}As$ curves lie lower than GaAs ones. However, this comparison assumes

equivalent initial surface roughnesses in strained and unstrained samples before phosphorus exposure. This is probably not the case: the strained sample would probably present long-range and smooth surface undulations, which cannot be detected by RHEED observations, in order to slightly relax the stored elastic energy. These undulations will favor the wirelike roughening which is observed on AFM views (Fig. 3). Let us note that for the unstrained samples X0 and X53 the roughening morphology is dotlike. On the other hand, AFM view of a $Ga_{0.3}In_{0.7}As$ film grown on an InP substrate and exposed to phosphorus also displays a wire-like morphology after roughening. Last, let us note that if the phosphorus incorporation was enhancing the average strain instead of reducing it (e.g., $Ga_{0.7}In_{0.3}As$ on InP), both roughening mechanisms would compete.

V. CONCLUSIONS

In this work we have studied the surface reactivity of $Ga_{1-x}In_xAs$ alloys to a phosphorus flux, and we have shown that for a 500 °C substrate temperature, except for the InAs case, the surface roughens rather rapidly and that roughening occurs more rapidly in the alloy case than in the GaAs one. These observations could not be attributed to different amounts of phosphorus incorporated in the layer, as determined by x-ray photoelectron spectroscopy (XPS). We have proposed a model which emphasizes the role of surface reconstruction, and more precisely of dimers: they tend to order the surface ternary (GaAsP, InAsP) or quaternary (GaInAsP) alloys, and thus govern the calculated phosphorus incorporation curves, which are in reasonable agreement with surface roughening observations. Valence force field calculations, taking properly into account the surface reconstruction, show that the difference between GaAs and InAs is related to the elastic energy differences occurring upon phosphorus incorporation in both systems. For the alloy matched to its substrate, the surface reconstruction, mainly dimers, induces some alloy ordering in the atomic layers very closed to the surface, which renders less favorable phosphorus incorporation (above half a monolayer) as far as surface keeps flat. In the case of strained alloys the roughening mechanism is completely different (large wires are used instead of initially small dots which ripen), and is related to initial smooth undulations of the strained alloy film. In this paper we have chosen to focus on roughening mechanisms, but we have also shown that this roughening can be experimentally avoided by making use of the kinetic limitations associated with lower substrate temperature.

ACKNOWLEDGMENTS

We wish to acknowledge Dominique Deresmes for AFM measurements, C. Coinon for his technical assistance in the MBE experiments, and D. Vignaud for a critical reading of this manuscript.

*Electronic address: catherine.priester@isen.fr

[1] M. Gerhardt, G. Kirpal, R. Schwabe, G. Benndorf, and V. Gottschalch, Thin Solid Films **392**, 85 (2001).

[2] R. Kudela, M. Kucera, B. Olejnikova, P. Elias, S. Hasenhrl, and J. Novak, J. Cryst. Growth **212**, 21 (2000).

[3] J.C. Garcia, P. Maurel, P. Bove, and J.P. Hirtz, J. Appl. Phys. **30**, 1186 (1991).

[4] W. Wu, S.L. Skala, J.R. Tucker, J.W. Lyding, A. Seabaugh, E.A. Beam III, and D. Jovanovic, J. Vac. Sci. Technol. A **13**, 602 (1995).

[5] O. Schuler, O. Dehaese, X. Wallart, and F. Mollot, J. Appl. Phys. **84**, 766 (1998).

[6] O. Dehaese, X. Wallart, O. Schuler, and F. Mollot, J. Appl. Phys. **84**, 2127 (1998).

[7] Y. Moon, T-W. Lee, S. Yoon, K. Yoo, and E. Yoon, J. Cryst. Growth **208**, 160 (2000).

[8] R. André, S. Wey, and C.W. Tu, J. Cryst. Growth **235**, 65 (2002).

[9] M. B. Panish and H. Temkin, *Gas Source Molecular Beamp Epitaxy: Growth and Properties of Phosphorus Containing III-V Heterostructures* (Springer, Berlin, 1993).

[10] M.J. Hafich, J.H. Quigley, R.E. Owens, G.Y. Robinson, D. Li, and N. Otsuka, Appl. Phys. Lett. **54**, 2686 (1989).

[11] S.W. Chiou, C.P. Lee, J.M. Hong, C.W. Chen, and Y. Tsou, J. Cryst. Growth **206**, 166 (1999).

[12] Y.K. Fukai, F. Hyuga, T. Nittono, K. Watanabe, and H. Sugahara, J. Vac. Sci. Technol. B **17**, 2524 (1999).

[13] Y. Moon and E. Yoon, J. Cryst. Growth **212**, 61 (2000).

[14] J.M. Moison, M. Bensoussan, and F. Houzay, Phys. Rev. B **34**, 2018 (1986).

[15] G. Hollinger, D. Gallet, M. Gendry, C. Santinelli, and P. Viktorovitch, J. Vac. Sci. Technol. B **8**, 832 (1990).

[16] C.H. Li, L. Li, D.C. Law, S.B. Visbeck, and R.F. Hicks, Phys. Rev. B **65**, 205322 (2002)

[17] S. Yoon, Y. Moon, T.W. Lee, E. Yoon, and Y.D. Kim, Appl. Phys. Lett. **74**, 2029 (1999).

[18] H. Yang, P. Ballet, and G. Salamo, J. Appl. Phys. **89**, R7871 (2001).

[19] J. Jönsson, F. Reinhardt, M. Zorn, K. Ploska, W. Richter, and J. Rumberg, Appl. Phys. Lett. **64**, 1998 (1994).

[20] K. Mahalingham, Y. Nakamura, N. Otsuka, H.Y. Lee, M.J. Hafich, and G.Y. Robinson, J. Electron. Mater. **21**, 129 (1992).

[21] A. Aurand, J. Leymarie, A. Vasson, M. Mesrine, J. Massies, and M. Leroux, J. Appl. Phys. **89**, 3775 (2001).

[22] H.H. Farrell and C.J. Palmstrom, J. Vac. Sci. Technol. B **8**, 903 (1990).

[23] W. Barvosa-Carter, R.S. Ross, C. Ratsch, F. Grosse, J.H.G. Owen, and J.J. Zinck, Surf. Sci. **499**, L129 (2002).

[24] M. Sauvage-Simkin, Y. Garreau, R. Pinchaux, M.B. Véron, J.P. Landesman, and J. Nagle, Phys. Rev. Lett. **75**, 3485 (1995).

[25] L. Bellaiche, K. Kunc, M. Sauvage-Simkin, Y. Garreau, and R. Pinchaux, Phys. Rev. B **53**, 7417 (1996).

[26] D.A. Shirley, Phys. Rev. B **5**, 4709 (1972).

[27] C.S. Fadley, Prog. Surf. Sci. **16**, 275 (1984).

[28] M. Seelmann-Eggebert and H.J. Richter, Phys. Rev. B **43**, 9578 (1991)

[29] G. Grenet, E. Bergignat, M. Gendry, M. Lapeyrade, and G. Hollinger, Surf. Sci. **352-354**, 734 (1996).

[30] J.J. Joyce, M. Del Guidice, and J.H. Weaver, J. Elec. Spectrosc. Relat. Phenom. **49**, 31 (1989).

[31] G. Le Lay, D. Mao, A. Kahn, Y. Hwu, and G. Margaritondo, Phys. Rev. B **43**, 14 301 (1991).
[32] P. Vogt, A.M. Frisch, Th. Hannapel, S. Visbeck, F. Willig, Ch. Jung, R. Follath, W. Braun, W. Richter, and N. Esser, Appl. Surf. Sci. **166**, 190 (2000).
[33] X. Wallart, Surf. Sci. **506**, 203 (2002).
[34] N. Esser, W.G. Schmidt, J. Bernholc, A.M. Frisch, P. Vogt, M. Zorn, M. Pristovsek, W. Richter, F. Bechstedt, Th. Hannapel, and S. Visbeck, J. Vac. Sci. Technol. B **17**, 1691 (1999).
[35] W.G. Schmidt, F. Bechstedt, N. Esser, M. Pristovsek, Ch. Schultz, and W. Richter, Phys. Rev. B **57**, 14 596 (1998).
[36] R.R. Lapierre, T. Okada, B.J. Robinson, D.A. Thompson, and G.C. Weatherly, J. Cryst. Growth **155**, 1 (1995).
[37] R.R. Lapierre, T. Okada, B.J. Robinson, D.A. Thompson, and G.C. Weatherly, J. Cryst. Growth **158**, 6 (1996).
[38] X. Wu and G.C. Weatherly, J. Cryst. Growth **233**, 88 (2001).
[39] S.B. Zhang and A. Zunger, Appl. Phys. Lett. **71**, 677 (1997).
[40] P.N. Keating, Phys. Rev. **145**, 637 (1966).
[41] R.M. Martin, Phys. Rev. B **1**, 4005 (1970).
[42] S.H. Wei, L.G. Ferreira, and A. Zunger, Phys. Rev. B **41**, 8240 (1990).
[43] *Numerical Data and Functional Relationships in Science and Technology*, edited by O. Madelung, M. Schultz, and H. Weiss, Landolt-Börnstein, New Series, Group III, Vol. 17 (Springer-Verlag, Berlin, 1982).
[44] Similar dimers effect on ordering has been previously described for bulk InGaP(100) alloys, see M. Zorn *et al.*, Phys. Rev. B **60**, 8185 (1999), and references therein.